Surveying the nucleon-nucleon momentum correlation function in the framework of quantum molecular dynamics model

Y. G. Ma,* Y. B. Wei, W. Q. Shen, X. Z. Cai, J. G. Chen, J. H. Chen, D. Q. Fang, W. Guo, C. W. Ma, G. L. Ma, Q. M. Su, W. D. Tian, K. Wang, T. Z. Yan, C. Zhong, and J. X. Zuo

Shanghai Institute of Applied Physics, Chinese Academy of Sciences, P.O. Box 800-204, Shanghai 201800, China

(Received 9 February 2005; published 23 January 2006)

Momentum correlation functions of nucleon-nucleon pairs are presented for reactions with C isotopes bombarding a ^{12}C target within the framework of the isospin-dependent quantum molecular dynamics model. The binding-energy dependence of the momentum correlation functions is also explored, and other factors that have an influence on momentum correlation functions are investigated. These factors include momentum-dependent nuclear equations of state, in-medium nucleon-nucleon cross sections, impact parameters, total pair momenta, and beam energy. In particular, the rise and the fall of the strength of momentum correlation functions at lower relative momentum are shown with an increase in beam energy.

DOI: 10.1103/PhysRevC.73.014604 PACS number(s): 25.10.+s, 25.70.Mn, 21.45.+v, 27.20.+n

I. INTRODUCTION

The method of two-particle intensity interferometry was developed by Hanbury Brown and Twiss (HBT) [1] in the early 1950s. Originally they applied a two-photon correlation to measure the angular diameter of stars and other astronomical objects. Initially, the method did not receive universal acceptance before a number of terrestrial experiments were performed to confirm it. Now the method of intensity interferometry is commonly referred to as the HBT effect. Although the original application of the HBT effect used photons as the detected particles, it was rapidly realized that the approach can be generalized to include correlation measurements for other bosons and fermions as well. The first measurements of the HBT effect in subatomic physics came from elementary-particle reactions. Goldhaber *et al.* extracted the spatial extent of an annihilation fireball in proton-antiproton reactions from two-pion correlations [2]. In fact, the method explores the idea that identical particles situated nearby in phase space experience quantum-statistical effects resulting from the (anti)symmetrization of the multiparticle wave function. For bosons, therefore, the two-particle coincidence rate shows an enhancement at a small momentum difference between the particles. The momentum range of this enhancement can be related to the size of the particle source in coordinate space. Recently, there has been not only substantial experimental literature on the technical applications, but also a large number of theoretical papers on momentum correlations with different models from low-energy to relativistic-energy heavy-ion collisions (HICs). For reviews, see Refs [3–6]. More recently, the HBT method was extended to others fields, for instance, the analogous correlations in semiconductors and in free space aiming at the fermionic statistics of electrons [7,8].

Many experimental measurements of the HBT effect have been made for HICs at intermediate energy in recent years. With an increase in beam energies, nucleon-nucleon (*NN*) collision plays a dominant role during the reaction process at intermediate energy, which results in the increasing importance of earlier particle emission. By application of the two-particle correlation function, one can obtain information on particle emission and collision dynamics.

In this energy domain, most correlation measurements focus on two-proton correlation functions. The shape of a two-proton correlation function reflects the combined effects of the Pauli blocking principle, Coulomb interaction, and proton-proton (*p*-*p*) nuclear interactions. Earlier measurements, performed by Lynch *et al.* [9], of two-proton correlation functions in intermediate-energy HICs provided the evidence for particle emission from localized highly excited regions. After that, many experimental groups investigated momentum correlation functions in various aspects, such as for unstable particle populations [10], the dependence on the impact parameter [11], the dependence of the total momentum of nucleon pairs [12], the dependence of the isospin of the emitting source [13], and so on. More interestingly, the HBT technique was used to construct a neutron-neutron (*n*-*n*) correlation function that is useful for investigating the properties of neutron-halo nuclei [14–16]. Details about the nuclear equation of state (EOS) and collision dynamics could be revealed from the correlation function by a comparison between experimental data and transport-model calculations.

However, in most studies of *p*-*p* correlation functions, the HBT strength at 20 MeV/*c* of the *p*-*p* relative momentum is taken as a unique quantity to determine the source size and/or emission time of two-proton emission. In a recent analysis for the HBT data below 100 MeV/nucleon with the imaging method, Verde *et al.* showed that the width of the correlation function provides the information on the source size of the fast dynamical component while the peak of the correlation function is sensitive to a relative yield from slow and fast emission components [17,18]. In addition, it was claimed that the proton emission from the slow statistical component was not suitably treated in the conventional transport model, such as the Boltzmann-Uehling-Uhlenback (BUU) model [19]. In light of the preceding studies, the whole shape on the correlation function is important for deducing space-time information of the emission source [17]. For heavy-ion reactions with

*Electronic address: ygma@sinap.ac.cn

a mid-heavy projectile and target combination in the Fermi energy domain, the slow-emission component should not be neglected. To minimize the complication of the slow and fast components of proton emission in correlation functions, it might be useful to choose light reaction systems at higher beam energies. In this context, we use a $C + {}^{12}C$ system to investigate momentum correlation functions above 100 MeV/nucleon in this work.

To understand the details of collisions for different reactions by the HBT studies, a reliable simulation of the collision dynamical process for heavy-ion reactions is required. The simulation gives a reasonable treatment of fragment formation after the final-state interaction. There are some good event-generator models that describe the collision process. In relativistic HICs, successful models include both the string-hadronic-like models, such as the relativistic quantum molecular dynamics (QMD) model and the parton cascade model. In the intermediate-energy region, the successful transport model includes the BUU model [20] and the QMD model [21]. From those event-generator models one can obtain the phase space of the emitted particles with different parameters of the EOS and then construct the momentum correlation function. Recently, the nuclear symmetry energy dependence of the HBT method was also explored through the isospin-dependent BUU model [22] in intermediate-energy HICs. Moreover, the nuclear binding-energy and separation-energy dependences of the HBT strength were investigated with the help of the isospin-dependent QMD (IDQMD) model [23,24]. In this paper, more features of momentum correlation functions are reported by use of the IDQMD model.

This paper is organized as follows: In Sec. II we describe the HBT technique and the IDQMD model; the stability of the IDQMD model is checked. Section III presents the results and discussions. We discuss the influences of the following factors: Initialization of projectile and target, emission time of nucleons, evolution time of the reaction, gate on the total momentum of the *NN* pair, soft-momentum-dependent (soft M) and stiff-momentum-dependent (stiff M) EOSs, in-medium *NN* cross sections, impact parameters, incident energy, etc. The conclusions are presented in Sec. IV.

II. HBT TECHNIQUE AND THE IDQMD MODEL

First, we recall the HBT technique. As we know, the wave function of relative motion of light identical particles is modified by the final-state interaction and quantum-statistical symmetries when they are emitted in close proximity in space and time, and this is the principle of intensity interferometry, i.e., the HBT method. In the standard Koonin-Pratt formalism [25–27], the two-particle correlation function is obtained by convolution of the emission function $g(\mathbf{p}, x)$, i.e., the probability for emitting a particle with momentum $\mathbf{p}$ from the space-time point $x = (\mathbf{r}, t)$ with the relative wave function of two particles:

$$C(\mathbf{P}, \mathbf{q}) = \frac{\int d^4x_1 d^4x_2 g(\mathbf{P}/2, x_1) g(\mathbf{P}/2, x_2) \, |\phi(\mathbf{q}, \mathbf{r})|^2}{\int d^4x_1 g(\mathbf{P}/2, x_1) \int d^4x_2 g(\mathbf{P}/2, x_2)}, \quad (1)$$

where $\mathbf{P}(= \mathbf{p}_1 + \mathbf{p}_2)$ and $\mathbf{q}[= \frac{1}{2}(\mathbf{p_1} - \mathbf{p_2})]$ are the total and relative momenta of the particle pair, respectively, and $\phi(\mathbf{q}, \mathbf{r})$ is the relative two-particle wave function with its relative position $\mathbf{r} = (\mathbf{r}_2 - \mathbf{r}_1) - \frac{1}{2}(\mathbf{v_1} + \mathbf{v_2})(t_2 - t_1)$. This approach is very useful in studying effects of a nuclear EOS and *NN* cross sections on the reaction dynamics of intermediate-energy HICs [5].

From the viewpoint of theoretical simulation, the correlation function can be established by an event generator that produces phase-space information by modeling the collision dynamics and particle production. The event-generator correlation functions are then constructed from the positions and momenta representing the single-particle emission distribution at the time of the last strong interaction, i.e., at freeze-out. In this work, the event generator is the IDQMD transport model [21], which has been successfully applied to HBT studies of HICs for neutron-rich nuclei-induced reactions [23,24]. Using Pratt's [28] computation code named CRAB (for correlation after burner), which takes into account final-state *NN* interactions, we evaluated two-nucleon correlation functions from the emission function given by the IDQMD model. In the following discussion, we introduce the model briefly.

The QMD approach is a many-body theory that describes heavy-ion reactions from intermediate energy to 2 GeV/nucleon [29]. It includes several important factors: Initialization of the target and the projectile, nucleon propagation in the effective potential, *NN* collisions in a nuclear medium, the Pauli blocking effect, and the numerical test. A general review of the QMD model can be found in [21]. The IDQMD model is based on the QMD model's embodiment the isospin factors.

The HIC dynamics at intermediate energies is governed mainly by three components: The mean field, two-body collisions, and Pauli blocking. Therefore, for an isospin-dependent reaction dynamics model, it is important to affiliate isospin degrees of freedom with the above three components. In addition, the sampling of phase space of neutrons and protons in the initialization should be treated separately because of the larger difference between neutron and proton density distributions for nuclei far from the β-stability line. For an exotic neutron-rich nucleus, one should sample a stable initialized nucleus with a neutron-skin or neutron-halo structure so that one can directly incorporate nuclear structure effects into a microscopic transport process. The IDQMD model has been improved based on the above ideas, and the details are subsequently given.

In the present calculations the interaction potential in the IDQMD is determined as follows:

$$U(\rho) = U^{\mathrm{Sky}} + V^{\mathrm{Coul}} + U^{\mathrm{sym}} + V^{\mathrm{Yuk}} + U^{\mathrm{MDI}} + U^{\mathrm{Pauli}}, \quad (2)$$

where U^{Sky} is the density-dependent Skyrme potential, and, when the momentum-dependent potential is include, it reads

$$U^{\mathrm{Sky}} = \alpha \left(\frac{\rho}{\rho_0}\right) + \beta \left(\frac{\rho}{\rho_0}\right)^{\gamma} + t_4 \ln^2 \left[\varepsilon \left(\frac{\rho}{\rho_0}\right)^{2/3} + 1\right] \frac{\rho}{\rho_0}, \quad (3)$$

TABLE I. The parameters of the interaction potentials.

α (MeV)	β (MeV)	γ	t_3 (MeV)	t_4 (MeV)	t_5 (MeV^{-2})	ε (MeV)	K (MeV)
−390.1	320.3	1.14	7.5	1.57	5×10^{-4}	21.54	200
−129.2	59.4	2.09	7.5	1.57	5×10^{-4}	21.54	380

where ρ and ρ_0 are the total nucleon density and its normal value, respectively. The parameters α, β, γ, t_4, and ε are related to the nuclear EOS and are listed in Table I. V_c is Coulomb potential, and U^{Yuk} is the Yukawa potential given by

$$U^{\mathrm{Yuk}} = t_3 \frac{\exp\left(\frac{|\overrightarrow{r_1} - \overrightarrow{r_2}|}{m}\right)}{\frac{|\overrightarrow{r_1} - \overrightarrow{r_2}|}{m}}, \tag{4}$$

where $m = 0.8$ fm. U^{MDI} is the momentum-dependent interaction [29]:

$$U^{\mathrm{MDI}} = t_4 \ln^2[t_5(\overrightarrow{p_1} - \overrightarrow{p_2})^2 + 1]\frac{\rho}{\rho_0}, \tag{5}$$

where $\overrightarrow{p_1}$ and $\overrightarrow{p_2}$ are the momenta of two interacting nucleons. U^{Pauli} is the Pauli potential:

$$U^{\mathrm{Pauli}} = V_p \left(\frac{\hbar}{p_0 q_0}\right)^3 \exp\left[-\frac{(\overrightarrow{r_i} - \overrightarrow{r_j})^2}{2q_0^2} - \frac{(\overrightarrow{p_i} - \overrightarrow{p_j})^2}{2p_0^2}\right]\delta_{p_i p_j}, \tag{6}$$

where

$$\delta_{p_i p_j} = \begin{cases} 1 \text{ for } n\text{-}n \quad \text{or} \quad p\text{-}p \\ 0 \text{ for } n\text{-}p. \end{cases}$$

The parameters V_p, p_0, and q_0 are 30 MeV, 400 MeV/c, and 5.64 fm, respectively. U^{sym} is the symmetry potential. In the present calculation, we use $U^{\mathrm{sym}} = C_{\mathrm{sym}}(\rho_n - \rho_p)/\rho_0\tau_z$, where C_{sym} is the strength of symmetry potential, taking the value of 32 MeV; ρ_n and ρ_p are the neutron density and the proton density, respectively; and τ_z is the zth component of the isospin degree of freedom, which equals 1 or −1 for neutrons or protons, respectively. The parameters of the interaction potential are given in Table I, where $K = 200$ or 380 MeV means the soft M or the stiff M potential, respectively.

The in-medium NN cross section can be parametrized as isospin dependent from the available experimental data. Studies of collective flow in HICs at intermediate energies revealed the reduction of the in-medium NN cross sections [30–32]. An empirical expression of the in-medium NN cross section [31] is used:

$$\sigma_{NN}^{\mathrm{med}} = \left(1 + f\frac{\rho}{\rho_0}\right)\sigma_{NN}^{\mathrm{free}}, \tag{7}$$

with the factor $f \approx -0.2$, which has been found to better reproduce the flow data [30]. Here $\sigma_{NN}^{\mathrm{free}}$ is the experimental NN cross section [33]. The free neutron-proton (n-p) cross section $\sigma_{NN}^{\mathrm{free}}$ is about a factor of 3 times larger than the free n-n or p-p cross section below about 400 MeV/nucleon in the laboratory energy. It should be mentioned that the relationship between the n-p cross section and n-n (p-p) cross section depends also on the modification of the nuclear density distributions during the reactions.

The Pauli blocking effect in the IDQMD model is treated separately for the neutron and the proton: Whenever a collision occurs, we assume that each nucleon occupies a six-dimensional sphere with a volume of $\hbar^3/2$ in the phase space (considering the spin degree of freedom), and then we calculate the phase volume V of the scattered nucleons being occupied by the rest nucleons with the same isospin as that of the scattered ones. We then compare $2V/\hbar^3$ with a random number and decide whether the collision is blocked.

When the initialization of the projectile and the target is taken in the IDQMD model, the density distributions of protons and neutrons are distinguished from each other. The references of neutron and proton density distributions for the initial projectile and target nuclei in the IDQMD model are taken from the Skyrme-Hartree-Fock (SHF) method with parameter set SKM*. Using this density distribution, we can get the initial coordinate of nucleons in nuclei in terms of the Monte Carlo sampling method. The momentum distribution of nucleons is generated by means of the local Fermi gas approximation:

$$P_F^i(\vec{r}) = \hbar[3\pi^2\rho_i(\vec{r})]^{\frac{1}{3}}, \quad (i = n, p). \tag{8}$$

In the model, the radial density can be written as

$$\rho(r) = \sum_i \frac{1}{(2\pi L)^{3/2}}\exp\left(-\frac{r^2 + r_i^2}{2L}\right)\frac{L}{2rr_i} \times \left[\exp\left(\frac{rr_i}{L}\right) - \exp\left(-\frac{rr_i}{L}\right)\right], \tag{9}$$

where L is the so-called Gaussian wave width (here $L = 2.16$ fm^2).

Stability of the initialized nucleus is checked by the time evolution of the system at zero temperature [24]. The accepted configurations are quite stable: Only a few percentage of nucleons escape from the nucleus until 200 fm/c in the intermediate-energy domain. In addition, we also check the stability by tracking the time evolutions of the average binding energy and the root-mean-square radius of the initialized nucleus, and good enough stability is found. Lighter nuclei are somewhat less stable. One or two out of ten nuclei lose a nucleon in the required time span. To avoid taking an unstable initialization of projectile and target in the IDQMD calculation, we select the initialization samples of only those nuclei that meet the required stability.

Nuclear fragments are constructed by a modified isospin-dependent coalescence model, in which particles with relative momentum smaller than $p_0 = 300$ MeV/c and relative distance smaller than $R_0 = 3.5$ fm will be combined into a cluster.

In our calculations, the reactions of C isotopes with ^{12}C are performed. Most simulations are done in head-on collisions ($b = 0$ fm) at 100 or 800 MeV/nucleon. The momentum correlation functions are constructed by the phase-space points at 200 fm/c when the system is basically at the freeze-out stage.

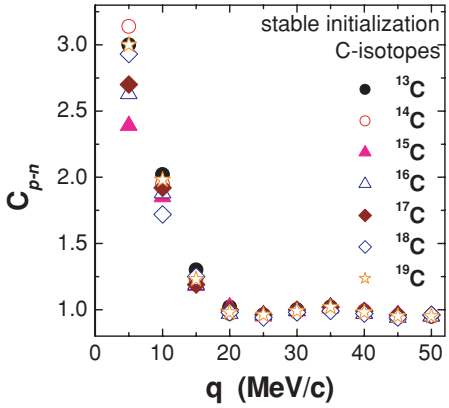

FIG. 1. (Color online) The p-n correlation functions $C_{p\text{-}n}$ for the reactions of a chain of C isotopes with ^{12}C at 800 MeV/nucleon and $b = 0$ fm by use of the stable initialization of projectile and target. The meanings of the symbols are given on the right-hand side of the figure.

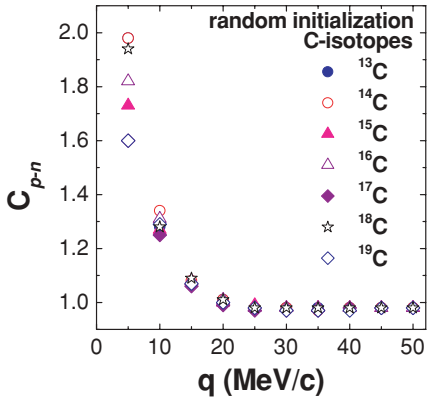

FIG. 3. (Color online) The p-n correlation function $C_{p\text{-}n}$ obtained for the reactions of a chain of C isotopes with a ^{12}C target at 800 MeV/nucleon by use of the random initialization of the projectile and the target. Symbols that represent the different isotopes are defined on the right-hand side of the figure.

III. RESULTS AND DISCUSSIONS

A. Stable initialization versus random initialization

Figure 1 shows proton-neutron (p-n) correlation functions from the reactions induced by a chain of C isotopes projected on the ^{12}C target at 800 MeV/nucleon of incident energy and head-on collisions (impact parameter $b = 0$ fm) when a suitable selection of the stable initialization is used. In this figure the HBT strength of each isotope at a lower relative momentum can be separated. If we plot this strength at 5 MeV/c ($C_{p\text{-}n}$) as a function of the mean binding energy (E_b) of the projectiles (C isotopes), we find that there exists an approximate linear relationship between $C_{p\text{-}n}$ and E_b, as shown by the filled circles in Fig. 2.

To investigate the importance of initialization in the HBT study, a comparison was performed with a random initialization for the projectile and the target in the IDQMD model based on Monte Carlo sampling. In random initialization, the phase space of the nucleons is generated with Monte Carlo random sampling. During sampling of each nucleon, if the distance between every two nucleons is larger than 1.5 fm and the product of the space radius and the momentum radius between two nucleons is larger than one constant according to the uncertainty relationship, the sampling will be accepted. In this case, there is no additional requirement of the binding energy of the projectile or the target.

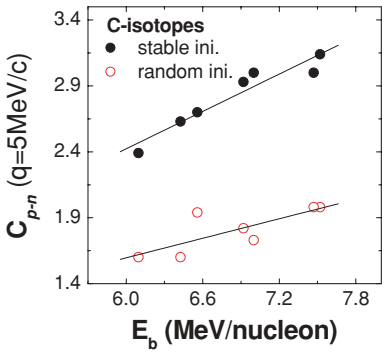

FIG. 2. (Color online) The relationship between the p-n correlation function $C_{p\text{-}n}$ at 5 MeV/c and the average binding energy per nucleon of C isotopes. The filled circles represent the results obtained with the stable initial phase space taking in the IDQMD model according to the SHF density distribution. The open circles represent the results with the random initial phase space. The collisions were simulated at 800 MeV/nucleon and $b = 0$ fm. The target is ^{12}C. The lines are linear fits to guide the eyes.

With such a random initialization, the initial phase space of the nucleons for the projectile and the target is different event by event. Through the transport process of the IDQMD model, we can obtain the momentum correlation function and extract the HBT strength in the final states. Figure 3 shows the p-n HBT strengths, for different C isotopes by randomly sampled initialization. Similar to that of Fig. 1, the strength at 5 MeV/c is not a constant for different isotope-induced reactions that are indicated by the open circles in Fig. 2. However, two apparent differences can be observed between the results of stable initialization and random initialization. One is the difference in the magnitude of the HBT strength. The values of $C_{p\text{-}n}$ at 5 MeV/c with the random initialization are less than those with the stable initialization. For the random initialization, the initial phase space, which may not meet the requirement of the ground state as required in the SHF calculation, fluctuates event by event. In this case the tightness of the initial nucleus becomes weaker than that with a stable initialization of the phase space that is sampled by the SHF density distribution. Thus the values of $C_{p\text{-}n}$ at 5 MeV/c that can embody the tightness between the nucleons become smaller. The other difference is the slope of $C_{p\text{-}n}$ vs. E_b. A steeper linear relationship is observed for the stable initial phase space, while the dependence of $C_{p\text{-}n}$ vs. E_b becomes weaker in the random case.

The comparison between both different initialization methods indicates that the reasonable initial phase space of the projectile that is sampled by the experimental E_b and the SHF density calculation in the IDQMD model is important and suitable for investigating the dependence of the binding energy for some observables. In the following calculations, we use

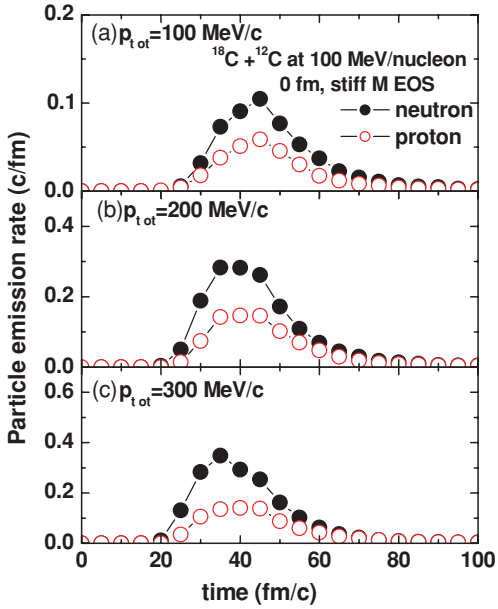

FIG. 4. (Color online) The time evolution of the emission rate of nucleons for ^{18}C + C at 100 MeV/nucleon and $b = 0$ fm with the different gates of the total *NN* pair momentum.

the stable initialization to study some features of momentum correlation functions.

B. Emission time of nucleons and evolution time of reaction

In the intermediate-energy domain, the extraction of the space-time information is further complicated by two effects. One is the presence of multiple sources of particle emission [34]; the other is the different time scale of statistical and dynamical emissions from equilibrium and nonequilibrium sources [17,18]. The total momentum-gated correlation function can be used to investigate the latter effects. Understanding the emission time sequence of neutrons and protons will be helpful for understanding the nuclear interaction. It also might be sensitive to the nuclear EOS. It has been shown that the emission times of the nucleons are related to their kinetic energies. Generally, earlier emitted nucleons have higher energies than later ones. Some results have been demonstrated in the experiments [35].

Figure 4 shows the time evolution of the particle emission rate by use of the Stiff M EOS. The open circles connected with solid curves show the proton emission rate and the filled ones represent the neutron emission rate. The collisions are simulated for ^{18}C + ^{12}C at 100 MeV/nucleon and $b = 0$ fm. In the following discussion, except for the special note, the collisions are all performed in the above circumstances.

From this figure, nucleons begin to be emitted around 20 fm/c, and their emission rates reach their maximum 15–20 fm/c later. With increasing total *NN* momentum $P_{\rm tot}$, the peak of the emission rate of nucleons becomes larger and its corresponding time tends to an earlier time. This indicates that nucleons with higher total pair momentum are emitted earlier. Higher momentum nucleons belong mostly to preequilibrium emission nucleons and essentially originate from higher-density regions. In contrast, lower-momentum nucleons are mostly emitted from equilibriumlike sources. For *n-p* pairs with lower total momentum, the emission rate of a neutron and a proton is almost synchronous, i.e., there is no obvious difference of the emission sequence between neutron and proton. However, for the *n-p* pair with larger total momentum, the emission rate of neutrons reaches the peak value earlier than that of protons; it means that, on average, neutrons are emitted earlier than protons. The reason why the emission rate of neutrons is larger than that of protons stems from the neutron-rich content of the projectile. Two interpretations seem to be possible. On the one hand, the symmetry potential term in Eq. (2) plays an important role in controlling the emission of nucleons. In a neutron-rich projectile-induced reaction, protons could feel a stronger attractive potential because of neighboring neutrons, which results in more bound protons for disassembling sources. On the other hand, neutrons will, on the one side, feel the stronger repulsive interaction because of more *n-n* pairs and, on the other side, feel smaller attractive potential because of the decreasing of the average assorted number of nearest-neighbor protons for a certain neutron for an increasing isospin of the source. For both reasons more unbound neutrons are produced for disassembling sources with higher isospins [36].

Experimentally, the momentum correlation function reflects the information in the final state of the reaction. Theoretically, the final state can be seen as the state at the freeze-out of the system. Since the HBT method is sensitive to the space-time information, we investigate the HBT method

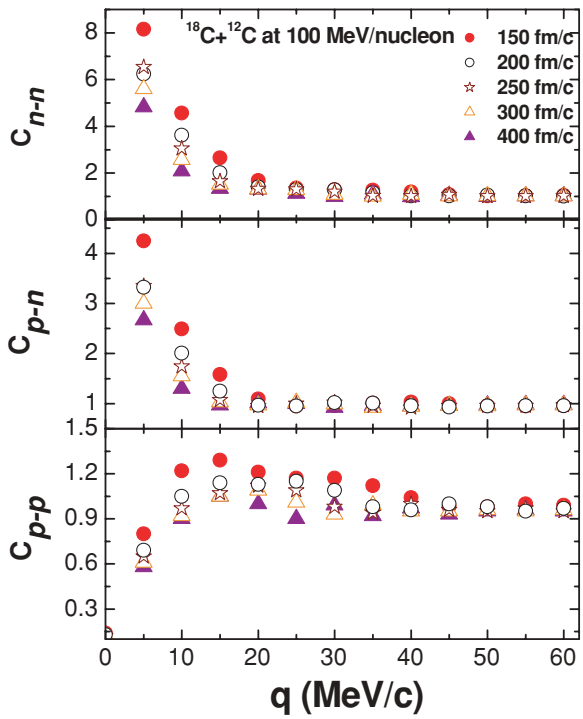

FIG. 5. (Color online) The momentum correlation functions of *n-n*, *p-n*, and *p-p* pairs for ^{18}C + C at 100 MeV/nucleon and $b = 0$ fm are constructed in different evolution times of the system. The evolution times are given in the top panel on the right-hand side.

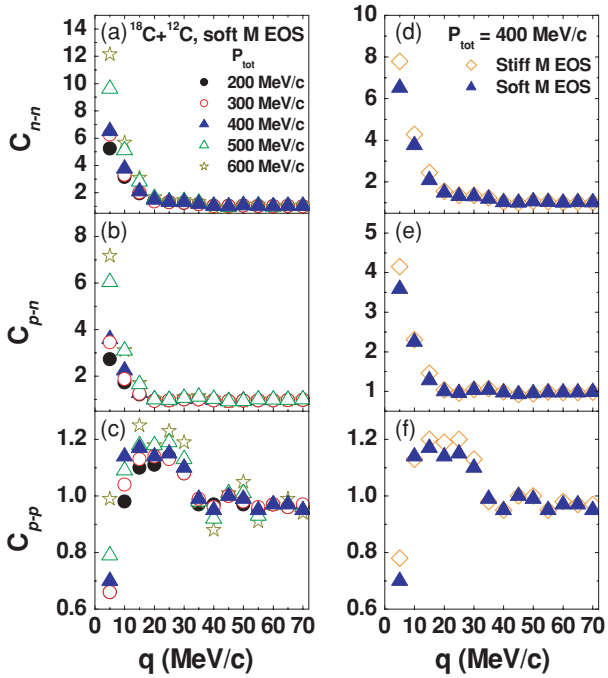

FIG. 6. (Color online) The two-nucleon correlation functions $C_{n\text{-}n}$, $C_{p\text{-}n}$, and $C_{p\text{-}p}$ for ^{18}C + C at 100 MeV/nucleon and $b = 0$ fm with the different total pair momenta ($P_{\rm tot}$) cuts or EOS parameters: The left-hand panels correspond to the different gates of $P_{\rm tot}$ while the right-hand panels correspond to different EOSs for $P_{\rm tot} =$ 400 MeV/c.

at different evolution times of reaction. Figure 5 shows the correlation functions of *n-n*, *p-n*, and *p-p* pairs when the evolution time of reaction $t = 150, 200, 250, 300$, and 400 fm/c.

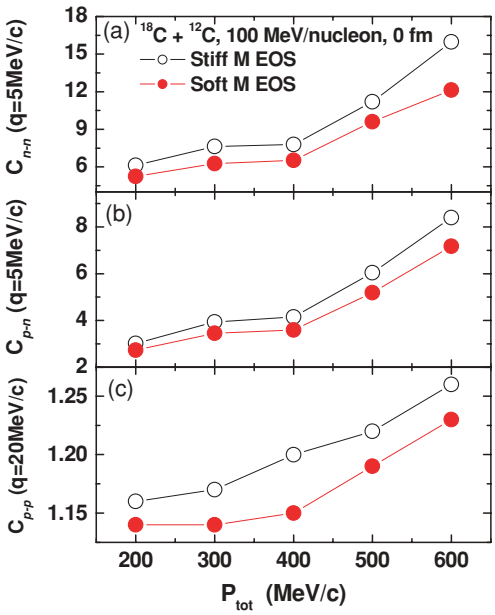

FIG. 7. (Color online) The HBT strength of two-nucleon correlation functions for *n-n* and *p-n* at 5 MeV/c or at *p-p* at 20 MeV/c for ^{18}C + C at 100 MeV/nucleon as a function of the gate of the total momentum ($P_{\rm tot}$) of the nucleon-nucleon pairs in the collisions.

Generally, HBT values become smaller in later evolution times because of the weakness of the *NN* correlation when the system is diluted. However, we can roughly say that the HBT values do not change dramatically after $t = 200$ fm/c compared with earlier times. Because of the limited computation resource, hereafter we investigate the features of the HBT values for all systems when $t = 200$ fm/c.

C. Gate of the total momentum

Since the magnitude of the total pair momentum is related to the nucleon emission time, we discuss the effect of the total pair momentum on the HBT results in this subsection. An earlier emission time induces a stronger correlation; a larger total momentum thus contributes to the strength of the correlation function too. We discuss the calculations with different total *NN* pair momentum ($P_{\rm tot}$) in what follows. The results are shown in Fig. 6. In this figure, three types of *NN* correlation functions, namely *n-n*, *n-p*, and *p-p*, are shown. From the left-hand panels, it is clearly observed that the higher the $P_{\rm tot}$, the higher the HBT value in lower relative momentum, whereas, from the right-hand panels, it is observed that HBT value in the region of lower relative momentum is higher with the soft M EOS than that with the stiff M EOS.

To see an overall trend of HBT strength versus $P_{\rm tot}$, we plot the value of $C_{n\text{-}n}$ ($C_{p\text{-}n}$) at 5 MeV/c or $C_{p\text{-}p}$ at 20 MeV/c as functions of $P_{\rm tot}$ in Fig. 7. The filled circles connected with the solid lines present the results with the soft M EOS and the open circles connected with the solid line show the ones with the stiff M EOS.

From the figure, it is clear that the strength of the two-nucleon correlation function is smaller at lower total pair momentum than that of the higher one. As is shown, the nucleons with lower total momenta are emitted later than those with higher total momenta, which naturally reduces the HBT strength. The calculated difference indicates the qualitative characterization of the emission process during the collisions. On the other hand, the tendency is similar despite the different combinations of *NN* pairs. Experimental results for the momentum-gated nucleon pairs show a trend similar to the one that can be found in the literature, see for example Refs. [11,12].

In addition, one can find that the HBT strength with the stiff M EOS is higher than that with the soft one. The influence of the different momentum-dependent EOSs on the HBT strength is discussed in the next subsection in detail.

D. Soft- and stiff-momentum-dependent potential

The EOS is considered an important property of nuclear matter and several studies have been made to investigate EOSs of finite nuclear matter [37]. In this section, we show the results of correlation functions with different EOS parameters.

In previous studies, the role of different potentials, i.e, the soft and the stiff potentials in transport models, has been investigated by means of some physical observables. However, in most cases, the potential does not include the momentum-dependent term, e.g., in HBT studies with isospin-dependent BUU model [22]. In this work we used

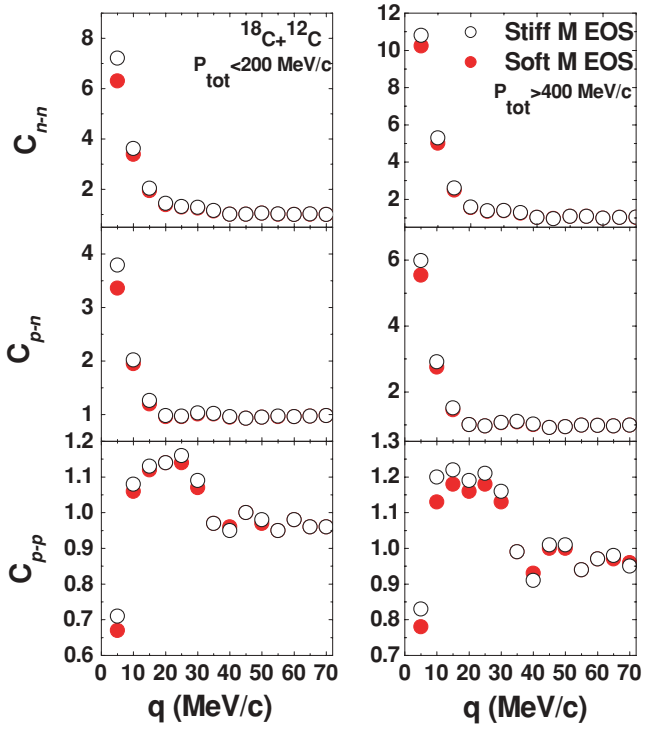

FIG. 8. (Color online) The comparison between the correlation function with soft M and stiff M EOSs for ^{18}C + C at 100 MeV/nucleon and $b = 0$ fm in IDQMD calculations. The left-hand panels correspond to the cases of $P_{\rm tot} < 200$ MeV/c while the right-hand panels correspond to the cases of $P_{\rm tot} > 400$ MeV/c. The filled and open circles represent the results with soft- and stiff-M EOSs, respectively.

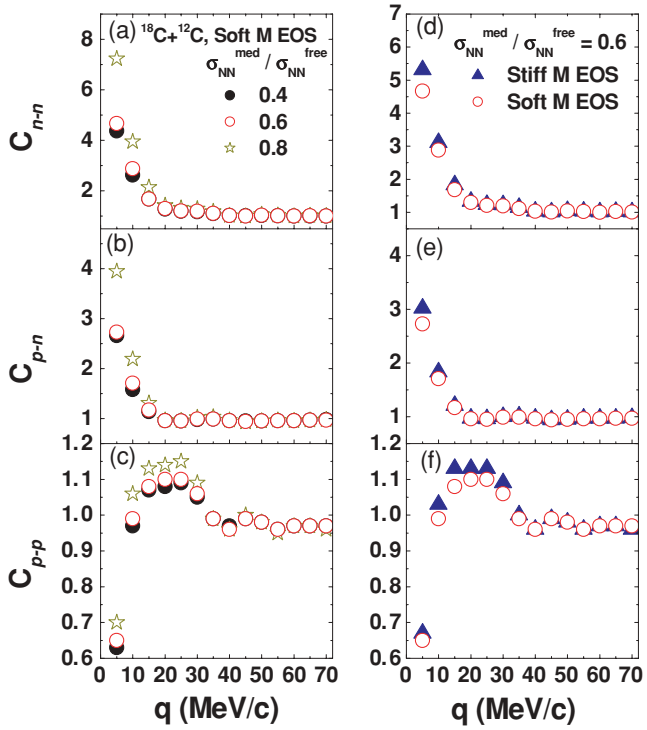

FIG. 9. (Color online) The two-nucleon correlation functions $C_{n\text{-}n}$, $C_{p\text{-}n}$ and $C_{p\text{-}p}$ for ^{18}C + C at 100 MeV/nucleon and $b = 0$ fm with different in-medium NN cross sections ($\sigma_{NN}^{\rm med}/\sigma_{NN}^{\rm free}$) (left-hand panels) or different EOSs (right-hand panels) for fixed $0.6\sigma_{NN}^{\rm free}$.

a momentum-dependent part in the potential, namely the soft M potential EOS and the stiff M potential EOS. We use also an isospin-dependent potential and calculated NN correlation functions with the above-mentioned two types of momentum-dependent potentials. The results are shown in Fig. 8.

In Fig. 8 the filled circles connected represent the correlation function with the soft M EOS and the open ones are the results with the the stiff M EOS. The left-hand panels are the HBT results with $P_{\rm tot} < 200$ MeV/c and the right-hand panels are the results with $P_{\rm tot} > 400$ MeV/c. From the figure, it is clear that the correlation function with the stiff potential is larger than that with the soft potential, which is similar to the calculation results with the BUU model [11]. The stiff potential makes the compression of nucleonic matter difficult compared with the case with the soft one and leads to a larger emission rate and earlier average emission time of nucleons, which in term leads to a stronger correlation function for the stiff potential.

E. In-medium nucleon-nucleon cross section

The effect of the in-medium NN cross section ($\sigma_{NN}^{\rm med}$) is discussed in this subsection. We use a value of $\sigma_{NN}^{\rm med}$, which is different from the free NN cross section ($\sigma_{NN}^{\rm free}$), to investigate its influence on momentum correlation functions. Figure 9 shows n-n, n-p, and p-p correlation functions for different $\sigma_{NN}^{\rm med}$ and EOSs. Slightly larger values of the HBT strength are found for larger $\sigma_{NN}^{\rm med}$, especially for 0.8 $\sigma_{NN}^{\rm free}$, as well as for the stiff M EOS. Figure 10 shows the HBT strengths at 5 MeV/c (for n-n and n-p) or at 20 MeV/c (for p-p) as functions of $\sigma_{NN}^{\rm med}$ in the stiff M and soft M EOSs. The strength increases with $\sigma_{NN}^{\rm med}$ and with the stiffness of the EOS. This can be understood by the following argument: With the increase in the in-medium NN cross section, the collision rate between two nucleons increases; consequently the system reaches the equilibrium stage faster. Before equilibrium is reached, more preequilibrium nucleons are emitted, which makes the strength of the correlation function larger.

F. Impact-parameter dependence

Considering the importance of the Wigner function that depends on the impact parameter, we investigate the momentum correlation function at different impact parameters. Collisions of ^{18}C + ^{12}C are performed at 100 MeV/nucleon and at the impact parameters of 0, 1, 2, 3, 4, and 5 fm. The calculated total momentum integrated correlation functions are shown in Fig. 11. Larger HBT values for central collisions or stiff EOSs are predicted. Their strengths are shown in Fig. 12.

In Ref. [11], some explanations of the effect of impact parameters have been presented. As we already know, the strength of the correlation function depends mainly on the

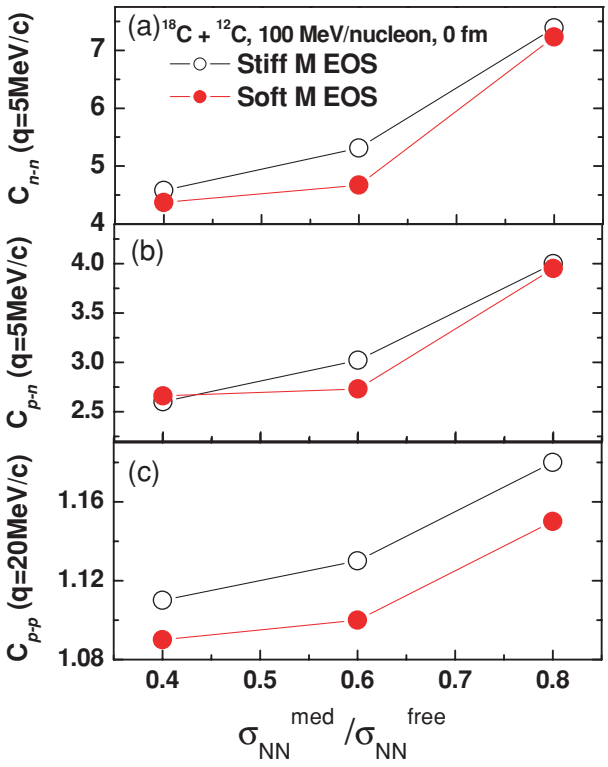

FIG. 10. (Color online) The HBT strengths of (a) *n-n* and *p-n* (b) pairs at 5 MeV/*c* and *p-p* pairs (c) at 20 MeV/*c* as functions of the in-medium *NN* cross section ($\sigma_{NN}^{med}/\sigma_{NN}^{free}$) from the reaction ^{18}C + ^{12}C at 100 MeV/nucleon and $b = 0$ fm. The open and filled symbols represent stiff M and soft M potentials, respectively.

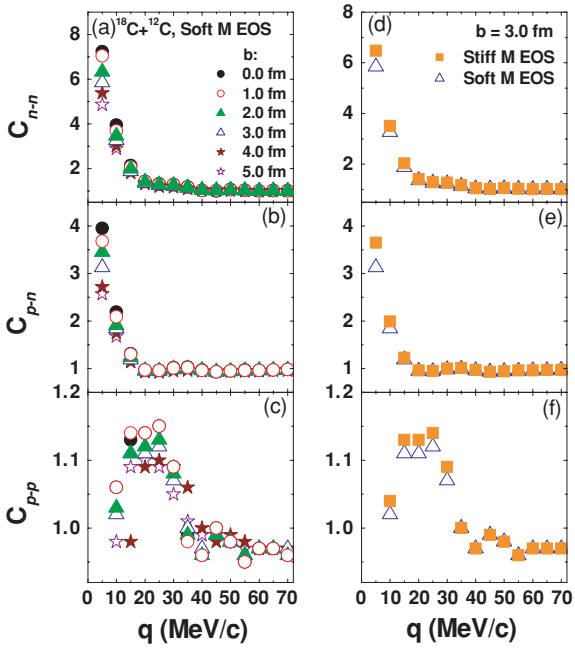

FIG. 11. (Color online) Momentum correlation functions for *n-n*, *p-n*, and *p-p* pairs are calculated in different impact parameters (left-hand panels) or with different EOSs at fixed $b = 3$ fm for ^{18}C + C at 100 MeV/nucleon.

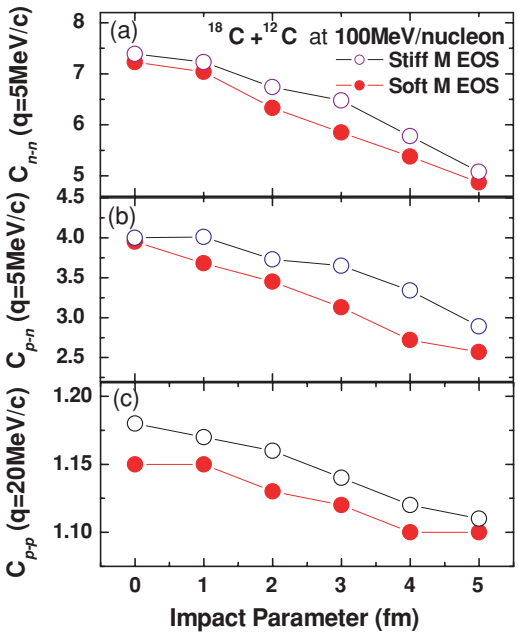

FIG. 12. (Color online) The strength of the *NN* correlation functions of (a) *n-n* and (b) *n-p* pairs at 5 MeV/*c* or (c) *p-p* pairs at 20 MeV/*c* for ^{18}C + C at 100 MeV/nucleon as functions of impact parameters. The open and filled symbols represent stiff M and soft M potentials, respectively.

emission time and the source size. From the figure, there exists a large difference between soft and stiff potentials. Second, the strength of a correlation function becomes weaker with an increasing impact parameter on both soft M and stiff M EOSs. This indicates that the stiffness of the potential in the IDQMD model does not change the tendency of the HBT strength with an increasing impact parameter. On the other hand, the behavior of the HBT strength with an impact parameter might reflect the changed size of the emitting source. In central collisions, *NN* collisions are very frequent, and emitted nucleons are mostly from one compact and hot, dense region. Therefore the HBT strength is larger because of the smaller source size, if compared with that of peripheral collisions. Some other factors, including Fermi jets, may also contribute to this effect [38].

G. Incident-energy dependence

The influence of incident energy on HBT strengths is investigated in this section. Figure 13 shows the momentum correlation functions at different beam energies (left-hand panels) and different EOSs (right-hand panels). Figure 14 displays the calculated HBT strengths of *n-n* [Fig. 14(a)], *p-n* [Fig. 14(b)], and *p-p* [Fig. 14(c)] pairs as a function of beam energy for head-on collisions. From the figure, both stiff M and soft M potentials provide a similar evolution of the HBT strength with beam energy. Interestingly, the HBT strength first increases with the incident energy and reaches a peak around 100 MeV/nucleon and then decreases at higher incident energies. The raise of the HBT strength at lower incident energies can be essentially attributed to drastic

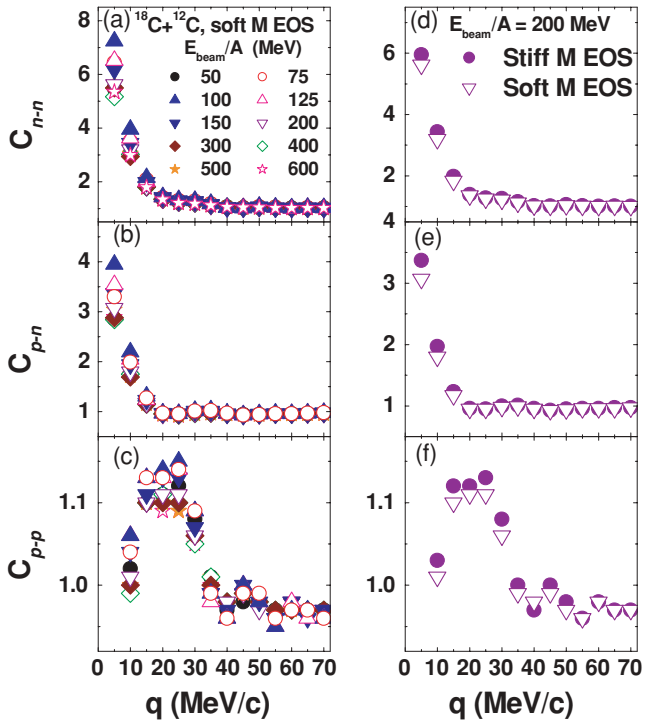

FIG. 13. (Color online) The momentum correlation functions of (a) *n-n*, (b) *p-n*, and (c) *p-p* pairs in different beam energies in head-on collisions for soft M EOSs (left-hand panels) or different EOSs at $E_{\text{beam}} = 200$ MeV/nucleon (right-hand panels).

NN collision at higher energies, which results, on average, in an earlier emission of nucleons. However, the decreasing

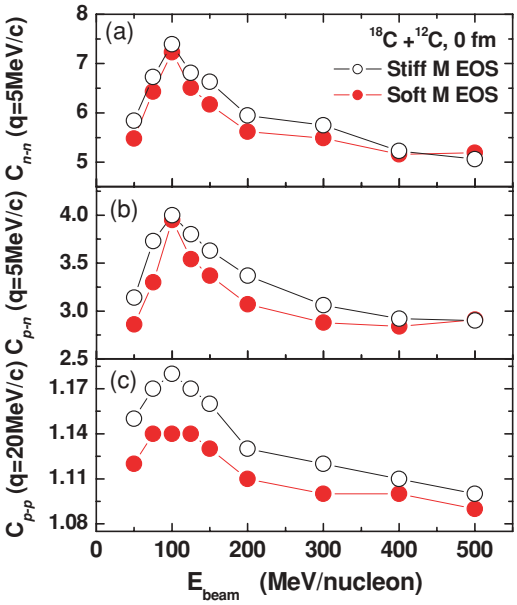

FIG. 14. (Color online) HBT strengths of (a) *n-n*, (b) *p-n*, and (c) *p-p* pairs as a function of beam energy in head-on collisions. Open and filled circles represent the calculations with stiff M or soft M potentials, respectively.

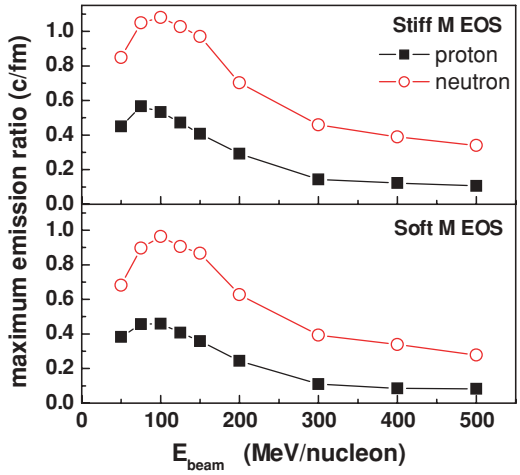

FIG. 15. (Color online) The maximum nucleon emission rate as a function of the incident energy. Squares and circles represent protons and neutrons, respectively.

behavior of HBT strengths with incident energies higher than 100 MeV/nucleon cannot be explained in this way.

To discuss the possible origin of the complex behavior of the HBT strength with incident energy, we investigate the maximum nucleon emission rate in the whole time evolution as a function of beam energy in Fig. 15. From the figure, the maximum nucleon emission rates show a rise and fall behavior similar to the one observed in Fig. 15 for the HBT strength. Around 100 MeV/nucleon, the nucleon emission rate is maximum. This energy coincides with the peak position of the HBT strength in Fig. 15. From this point of view, the HBT strength could be correlated to the maximum nucleon emission rate during HICs. The higher the nucleon emission rate, the stronger the HBT strength. Of course, another possible explanation for the falling branch of HBT strength can be attributed to the source size in the final state ($t = 200$ fm/c). It is expected that, in the energy range of a few hundreds of MeV/nucleon, where the repulsive *NN* interaction is dominant, a more dilute system might develop after freeze-out. Therefore the fall of the HBT with a beam energy above 100 MeV/nucleon indicates that the source size has been much expanded in the final state at higher energies. In contrast, the attractive mean field competes with the repulsive *NN* interaction below 100 MeV/nucleon. Shorter emission times with increasing beam energies may play a dominant role in determining the behavior of the HBT strength. Figure 15 also illustrates that the emission rate of neutrons is larger than that of protons and that the neutrons are emitted earlier than protons.

IV. SUMMARY

In summary, IDQMD model has been used as an event-generator to study the momentum correlation functions of *n-n*, *p-p*, and *n-p* pairs for C + ^{12}C. An approximate linear relationship between the strength of a correlation function at low relative momentum and the mean binding energy of projectiles has been revealed, and the influence of the

different initialization methods of the projectiles on momentum correlation functions has been also investigated. In addition, some different physical factors that have effects on momentum correlation functions have been shown in this work. These factors include nuclear EOSs and in-medium *NN* cross sections. It shows that the stiff M EOS or a larger in-medium *NN* cross section results in a stronger HBT strength than does the soft M EOS or a smaller in-medium *NN* cross section. Some other aspects that also have effects on momentum correlation functions, including the time evolution of the reaction system, the impact parameter, the gate of the total momenta of *NN* pairs, and the incident energy, are also explored. Results show that the HBT strength decreases with an increasing impact parameter because of an earlier emission or a compact source size in central collisions. A positive correlation between the gate of total *NN* pair momentum and the HBT strength can be explained by the earlier emission time of nucleons with higher total momentum. The rise and fall of the HBT strengths with the beam energy can be interpreted either in terms of the maximum nucleon emission rates during HICs or in terms of the dominant shorter emission time with an increasing beam energy below 100 MeV/nucleon and the larger later-stage expansion of the source size with an increasing beam energy above 100 MeV/nucleon.

ACKNOWLEDGMENTS

This work was supported in part by the Shanghai Development Foundation for Science and Technology under grant nos. 05XD14021 and 03 QA 14066, by the National Natural Science Foundation of China under grant nos. 10328259, 10135030, and 10535010, and by the Major State Basic Research Development Program under contract no. G200077404.

[1] R. Hanbury Brown and R. Q. Twiss, Nature (London) **178**, 1046 (1956).
[2] G. Goldhaber, S. Goldhaber, W. Lee, and A. Pais, Phys. Rev. **120**, 300 (1960).
[3] U. Heinz and B. Jacak, Annu. Rev. Nucl. Part. Sci. **49**, 529 (1999).
[4] D. H. Boal, C. K. Gelbke, and B. K. Jennings, Rev. Mod. Phys. **62**, 553 (1990).
[5] W. Bauer, C. K. Gelbke, and S. Pratt, Annu. Rev. Nucl. Part. Sci. **42**, 77 (1992).
[6] U. A. Wiedemann and U. Heinz, Phys. Rep. **319**, 145 (1999).
[7] M. Henny, S. Oberholzer, C. Strunk, T. Heinzel, K. Ensslin, M. Holland, and C. Schönenberger, Science **284**, 296 (1999); W. D. Oliver, J. Kim, R. C. Liu, and Y. Yamamoto, *ibid.* **284**, 299 (1999).
[8] R. de-Picciotto, M. Reznikov, M. Heiblum, V. Umansky, G. Bunin, and D. Mahalu, Nature (London) **389**, 162 (1997).
[9] W. G. Lynch, C. B. Chitwood, M. B. Tsang, D. J. Fields, D. R. Klesch, C. K. Gelbke, G. R. Young, T. C. Awes, R. L. Ferguson, F. E. Obenshain, F. Plasil, R. L. Robinson, and A. D. Panagiotou, Phys. Rev. Lett. **51**, 1850 (1983).
[10] J. Pochodzalla, C. K. Gelbke, W. G. Lynch, M. Maier, D. Ardouin, H. Delagrange, H. Doubre, C. Grégoire, A. Kyanowski, W. Mittig, A. Péghaire, J. Péter, F. Saint-Laurent, B. Zwieglinski, G. Bizard, F. Lefébvres, B. Tamain, J. Quebert, Y. P. Viyogi, W. A. Friedman, and D. H. Boal, Phys. Rev. C **35**, 1695 (1987).
[11] W. G. Gong, W. Bauer, C. K. Gelbke, and S. Pratt, Phys. Rev. C **43**, 781 (1991).
[12] N. Colonna, D. R. Bowman, L. Celano, G. D'Erasmo, E. M. Fiore, L. Fiore, A. Pantaleo, V. Paticchio, G. Tagliente, and S. Pratt, Phys. Rev. Lett. **75**, 4190 (1995).
[13] R. Ghetti, V. Avdeichikov, B. Jakobsson, P. Golubev, J. Helgesson, N. Colonna, G. Tagliente, H. W. Wilschut, S. Kopecky, V. L. Kravchuk, E. W. Anderson, P. Nadel-Turonski, L. Westerberg, V. Bellini, M. L. Sperduto, and C. Sutera, Phys. Rev. C **69**, 031605(R) (2004).
[14] N. A. Orr, Nucl. Phys. **A616**, 155 (1997).
[15] F. M. Marques, M. Labiche, N. A. Orr, J. C. Angélique, L. Axelsson, B. Benoit, U. C. Bergmann, M. J. G. Borge, W. N. Catford, S. P. G. Chappell, N. M. Clarke, G. Costa, N. Curtis, A. D'Arrigo, F. de Oliveira Santos, E. de Góes Brennand, O. Dorvaux, M. Freer, B. R. Fulton, G. Giardina, C. Gregorie, S. Grévy, D. Guillemaud-Mueller, F. Hanappe, B. Heusch, B. Jonson, C. Le Brun, S. Leenhardt, M. Lewitowicz, M. J. López, K. Markenroth, M. Motta, A. C. Mueller, T. Nilsson, A. Ninane, G. Nyman, I. Piqueras, K. Riisager, M. G. Saint Laurent, F. Sarazin, S. M. Singer, O. Sorlin, and L. Stuttgé, Phys. Lett. **B476**, 219 (2000).
[16] F. M. Marques, M. Labiche, N. A. Orr, J. C. Angélique, L. Axelsson, B. Benoit, U. C. Bergmann, M. J. G. Borge, W. N. Catford, S. P. G. Chappell, N. M. Clarke, G. Costa, N. Curtis, A. D'Arrigo, E. de Góes Brennand, F. de Oliveira Santos, O. Dorvaux, G. Fazio, M. Freer, B. R. Fulton, G. Giardina, S. Grévy, D. Guillemaud-Mueller, F. Hanappe, B. Heusch, B. Jonson, C. Le Brun, S. Leenhardt, M. Lewitowicz, M. J. López, K. Markenroth, A. C. Mueller, T. Nilsson, A. Ninane, G. Nyman, I. Piqueras, K. Riisager, M. G. Saint Laurent, F. Sarazin, S. M. Singer, O. Sorlin, and L. Stuttgé, Phys. Rev. C **64**, 061301(R) (2001).
[17] G. Verde, D. A. Brown, P. Danielewicz, C. K. Gelbke, W. G. Lynch, and M. B. Tsang, Phys. Rev. C **65**, 054609 (2002).
[18] G. Verde, P. Danielewicz, D. A. Brown, W. G. Lynch, C. K. Gelbke, and M. B. Tsang, Phys. Rev. C **67**, 034606 (2003).
[19] D. O. Handzy, W. Bauer, F. C. Daffin, S. J. Gaff, C. K. Gelbke, T. Glasmacher, E. Gualtieri, S. Hannuschke, M. J. Huang, G. J. Kunde, R. Lacey, T. Li, M. A. Lisa, W. J. Llope, W. G. Lynch, L. Martin, C. P. Montoya, R. Pak, G. F. Peaslee, S. Pratt, C. Schwarz, N. Stone, M. B. Tsang, A. M. Vander Molen, G. D. Westfall, J. Yee, and S. J. Yennello, Phys. Rev. Lett. **75**, 2916 (1995).
[20] G. F. Bertsch and S. Das Gupta, Phys. Rep. **160**, 189 (1988).
[21] J. Aichelin, Phys. Rep. **202**, 233 (1991).

[22] L. W. Chen, V. Greco, C. M. Ko, and B. A. Li, Phys. Rev. C **68**, 014605 (2003).
[23] Y. B. Wei, Y. G. Ma, W. Q. Shen, G. L. Ma, K. Wang, X. Z. Cai, C. Zhong, W. Guo, and J. G. Chen, Phys. Lett. **B586**, 225 (2004).
[24] Y. B. Wei, Y. G. Ma, W. Q. Shen, G. L. Ma, K. Wang, X. Z. Cai, C. Zhong, W. Guo, J. G. Chen, D. Q. Fang, W. D. Tian, and X. F. Zhou, J. Phys. G **30**, 2019 (2004).
[25] S. E. Koonin, Phys. Lett. **B70**, 43 (1977).
[26] S. Pratt, Phys. Rev. Lett. **53**, 1219 (1984).
[27] S. Pratt and M. B. Tsang, Phys. Rev. C **36**, 2390 (1987).
[28] S. Pratt, Nucl. Phys. **A566**, 103c (1994).
[29] J. Aichelin, A. Rosenhauer, G. Peilert, H. Stoecker, and W. Greiner, Phys. Rev. Lett. **58**, 1926 (1987).
[30] G. D. Westfall, W. Bauer, D. Craig, M. Cronqvist, E. Gaultieri, S. Hannuschke, D. Klakow, T. Li, T. Reposeur, A. M. Vander Molen, W. K. Wilson, J. S. Winfield, J. Yee, S. J. Yennello, R. Lacey, A. Elmaani, J. Lauret, A. Nadasen, and E. Norbeck, Phys. Rev. Lett. **71**, 1986 (1993).
[31] D. Klakow, G. Welke, and W. Bauer, Phys. Rev. C **48**, 1982 (1993).
[32] Y. G. Ma, W. Q. Shen, J. Feng, and Y. Q. Ma, Phys. Rev. C **48**, R1492 (1993); Y. G. Ma and W. Q. Shen, *ibid*. **51**, 3256 (1995).
[33] K. Chen, Z. Fraenkel, G. Friedlander, J. R. Grover, J. M. Miller, and Y. Shimamoto, Phys. Rev. **166**, 949 (1968).
[34] R. Ghetti, J. Helgesson, N. Colonna, B. Jakobsson, A. Anzalone, V. Bellini, L. Carlén, S. Cavallaro, L. Celano, E. De Filippo, G. DErasmo, D. Di Santo, E. M. Fiore, A. Fokin, M. Geraci, F. Giustolisi, A. Kuznetsov, G. Lanzanó, D. Mahboub, S. Marrone, F. Merchez, J. Martensson, F. Palazzolo, M. Palomba, A. Pantaleo, V. Paticchio, G. Riera, M. L. Sperduto, C. Sutera, G. Tagliente, M. Urrata, and L. Westerberg (CHIC Collaboration), Phys. Rev. C **64**, 017602 (2001).
[35] R. Ghetti, J. Helgesson, V. Avdeichikov, P. Golubev, B. Jakobsson, N. Colonna, G. Tagliente, S. Kopecky, V. L. Kravchuk, H. W. Wilschut, E. W. Anderson, P. Nadel-Turonski, L. Westerberg, V. Bellini, M. L. Sperduto, and C. Sutera, Phys. Rev. Lett. **91**, 092701 (2003).
[36] Y. G. Ma, Q. M. Su, W. Q. Shen, D. D. Han, J. S. Wang, X. Z. Cai, D. Q. Fang, and H. Y. Zhang, Phys. Rev. C **60**, 024607 (1999).
[37] P. Danielewicz, R. Lacey, and W. G. Lynch, Science **298**, 1592 (2002).
[38] H. Fuchs and K. Mohing, Rep. Prog. Phys. **57**, 231 (1994) and references therein.